MECHANIKA TEORETYCZNA
I STOSOWANA
Journal of Theoretical
and Applied Mechanics
4, 32, 1994

WAKE STRUCTURE AND GEOMETRY OF THE VORTEX PATH BEHIND MOVING CIRCULAR CYLINDER

ANDRZEJ BOGUSŁAWSKI

JANUSZ W.ELSNER

Institute of Thermal Machinery

University of Częstochowa

The paper describes the experiment undertaken in order to explain interaction betwen the Karman vortex street and a viscous wake behind the moving cylinder.

1. Introduction

The most characteristic feature of the flow in turbomachines, apart from its high turbulence level, is significant periodicity of a velocity field induced by the relative motion of both the blade rows of a turbine stage. This phenomenon, known in literature (cf Greitzer (1985), Gallus (1987)) as a rotor-stator interaction, has a major influence on the overall performance of turbomachines, so its effect has been thoroughly examined in many scientific centers. A review of the most important investigations in this field has been among others provided by Greitzer (1985) and Gallus (1987).

One of the essential aspects of the rotor-stator interaction, namely the effect of the flow pattern in stationary blading, has, in turn, been studied by Schultz et al.(1990). In order to generate the periodic wakes when simulating the action of the upstream blade row, they have used a row of cylindrical rods rotating in front of an annular cascade. Application of such a device for generation of an unsteady flow provokes a question: to what extent the flow pattern in viscous wakes behind periodically moving cylinders is affected by the Karman vortex path. There are a lot of experimental as well as theoretical studies on the vortex street behind motionless (cf Morkovin (1964)), vibrating

(cf Griffin and Ramberg (1974); Griffin and Hall (1991)) or rotating (cf Kimura et al. (1992)) cylinders, but to the best of authors knowledge there is no information concerning the interference of such two periodic flow phenomena. An attempt to study that effect has been therefore undertaken in this work.

2. Experimental set-up and signal processing

A scheme of the experimental facility is presented in Fig.1a. A disc of the radius $R_0 = 99$ mm with $z = 10$ cylindrical rods, each of them having the length $l = 90$ mm and diameter $d = 3$ mm, rotates at a speed $n = \text{const}$ in the plane perpendicular to the wind-tunnel axis. The wind tunnel nozzle with the outlet diameter $D = 80$ mm ensures a uniform radial velocity distribution $C(r) = \text{const}$ at the exit plane and in the flow region occupied by the jet potential core (Fig.1b).

The measurements of the flow-field has been taken in 5 control planes $x = \text{const}$ perpendicular to the jet axis within the range $x \leq 0.56D$. In each measuring section a DISA X hot-wire probe has traversed the velocity field along the arcs determined by the rotor mid span radius $R = R_0 + l/2 = 144$ mm (Fig.1c) and crossing the jet axis.

The voltages from both the channels of the hot-wire anemometer have been sampled via the 12-bit A/D converter at the rate $f_{samp} = 8$ kHz. Utilizing the reluctance transducer, the system has operated in the external trigger mode so that the data acquisition could be synchronized with the instantaneous rotor position. The signal from the transducer, formed in TTL-standard by the pulse shaper, has also been recorded during experiment in order to get the reference signal for the phase-averaging procedure.

At a fixed point of a statistically steady flow-field the instantaneous values of both the axial C_a and the circumferential C_u absolute velocity components may be expressed by a triple decomposition

$$\begin{aligned} C_a(t) &= \overline{C}_a + \tilde{C}_a(t) + c'_a(t) \\ C_u(t) &= \overline{C}_u + \tilde{C}_u(t) + c'_u(t) \end{aligned} \tag{2.1}$$

which consists of mean $\overline{C}$, periodic $\tilde{C}$ and random c' quantities, respectively.

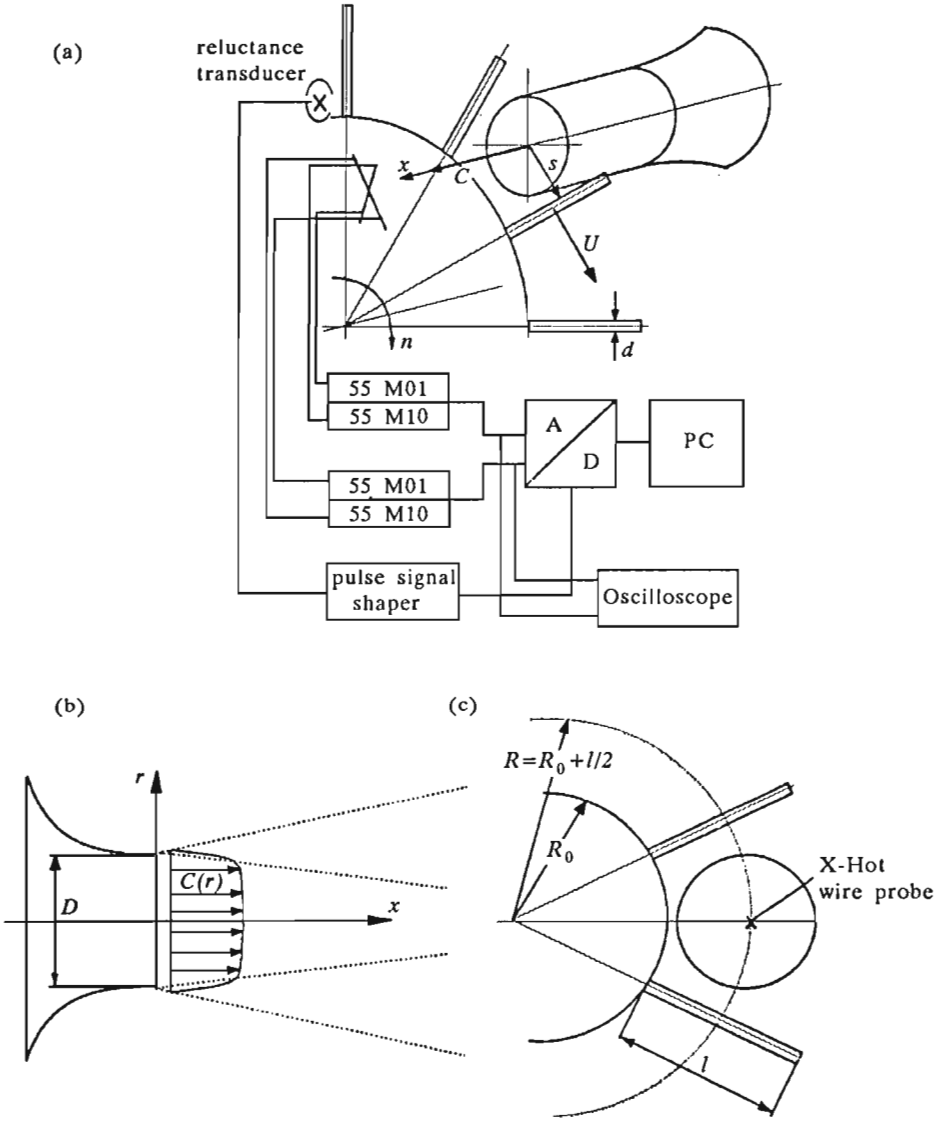

Fig. 1. Scheme of the experimental set-up; 55MO1 – DISA Main Unit, 55M10 – DISA CTA Standard Bridge

The phase-locked averaging procedure (cf Elsner (1987)) based on the relationships

$$
\begin{aligned}
<C_a(t)> &= \overline{C}_a + \tilde{C}_a(t) + \frac{1}{N}\sum_{i=1}^{N} C_a(t+\mathrm{i}T) \\
<C_u(t)> &= \overline{C}_u + \tilde{C}_u(t) + \frac{1}{N}\sum_{i=1}^{N} C_u(t+\mathrm{i}T)
\end{aligned}
\tag{2.2}
$$

where $T = 60/zn$, rejects the background turbulence and extracts only the deterministic motion from the total signal. Thus, taking into account (2.2) in (2.1) and introducing a nondimensional time coefficient $\tau = t/T$ ($t \in (0,T)$, $\tau \in (0,1)$), one may get the mean, periodic and random velocity components, respectively

$$
\begin{aligned}
\overline{C}_a &= \int_0^1 <C_a(\tau)> \, d\tau \\
\overline{C}_u &= \int_0^1 <C_u(\tau)> \, d\tau
\end{aligned}
\tag{2.3}
$$

$$
\begin{aligned}
\tilde{C}_a(\tau) &= <C_a(\tau)> - \overline{C}_a \\
\tilde{C}_u(\tau) &= <C_u(\tau)> - \overline{C}_u
\end{aligned}
\tag{2.4}
$$

$$
\begin{aligned}
C'_a(\tau+\mathrm{i}) &= C_a(\tau+\mathrm{i}) - <C_a(\tau)> \\
C'_u(\tau+\mathrm{i}) &= C_u(\tau+\mathrm{i}) - <C_u(\tau)>
\end{aligned}
\tag{2.5}
$$

The results obtained this way allow one to determine the corresponding velocity variances

$$
\begin{aligned}
\overline{\tilde{C}_a^2} &= \int_0^1 \tilde{C}_a^2(\tau)\, d\tau \\
\overline{\tilde{C}_u^2} &= \int_0^1 \tilde{C}_u^2(\tau)\, d\tau
\end{aligned}
\tag{2.6}
$$

$$\overline{C_a'^2} = \frac{1}{N}\sum_{i=1}^{N}\int_0^1 \left[C_a(\tau+\mathrm{i}) - \langle C_a(\tau)\rangle\right]^2 d\tau$$

$$\overline{C_u'^2} = \frac{1}{N}\sum_{i=1}^{N}\int_0^1 \left[C_u(\tau+\mathrm{i}) - \langle C_u(\tau)\rangle\right]^2 d\tau \tag{2.7}$$

3. Geometry of the vortex path behind moving circular cylinder

For the sake of preliminary interpretation of experimental results let us focus our attention on the vortex trajectories behind a cylinder moving in a 2D flow field. Fig.2 shows schematically a relative velocity profile with a first vortex formed on the "upper" side of a cylinder. For simplicity of further consideration let us also assume that a vortex center determines the origin of the Cartesian coordinate system x, y.

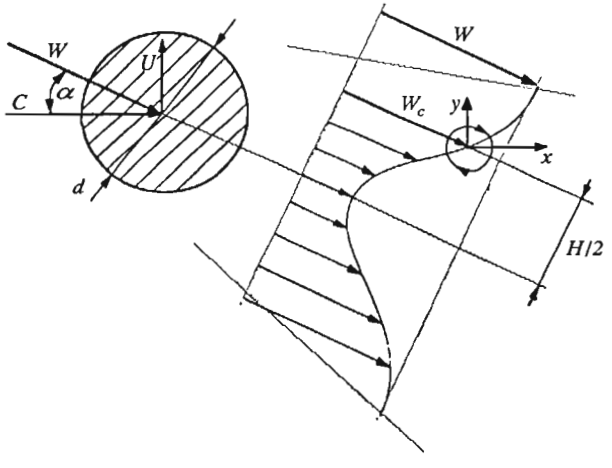

Fig. 2. Velocity profile in a relative motion behind moving cylinder

The characteristic Karman vortex frequency f_k may be calculated from the Strouhal number St based on cylinder diameter d and relative velocity W

$$F_k = \frac{\mathrm{St}W}{d} = \frac{\mathrm{St}}{d}\sqrt{U^2 + C^2} \tag{3.1}$$

Vortex convection velocity in a relative flow field reads

$$W_c = (1-k)W \tag{3.2}$$

where coefficient k may generally be a certain, a priori unknown function of time. Thus, the convection velocity components in a stationary frame of reference may be expressed as follows

$$\begin{aligned} (C_u)_c &= -W_c \sin\alpha + U \\ (C_a)_c &= W_c \cos\alpha \end{aligned} \tag{3.3}$$

Since

$$\begin{aligned} \sin\alpha &= \frac{U}{W} = \frac{U}{\sqrt{U^2+C^2}} = \frac{1}{\sqrt{1+\varphi^2}} \\ \cos\alpha &= \frac{C}{W} = \frac{C}{\sqrt{U^2+C^2}} = \frac{\varphi}{\sqrt{1+\varphi^2}} \end{aligned} \tag{3.4}$$

where velocity ratio $\varphi = C/U$, we finally have

$$(C_u)_c = kU \qquad (C_a)_c = (1-k)C \tag{3.5}$$

In a stationary coordinate system x, y a trajectory of the first vortex shown in Fig.2 may be represented by the parametric equation

$$\begin{aligned} x &= (C_a)_c t = (1-k)Ct \\ y &= (C_u)_c t = kUt \end{aligned} \tag{3.6}$$

If one assumes that the convection velocity is constant in space and time, what corresponds to the constant value of coefficient k, then it is easy to find that the Karman vortices travel in a flow field along the straight lines which form an angle β with the x-axis (Fig.3). Where

$$\beta = \arctan\frac{(C_u)_c}{(C_a)_c} = \arctan\Big(\frac{U}{C}\frac{k}{1-k}\Big) = \arctan\Big(\frac{1}{\varphi}\frac{k}{1-k}\Big) \tag{3.7}$$

Now, it is clear that the flow-region behind a moving rod will be covered by a set of parallel trajectories described by the equations

$$\begin{aligned} y^+ &= x\tan\beta + (\mathrm{i}-1)UT_k \\ y^- &= x\tan\beta + \Delta y_b + (\mathrm{i}-1)UT_k \end{aligned} \tag{3.8}$$

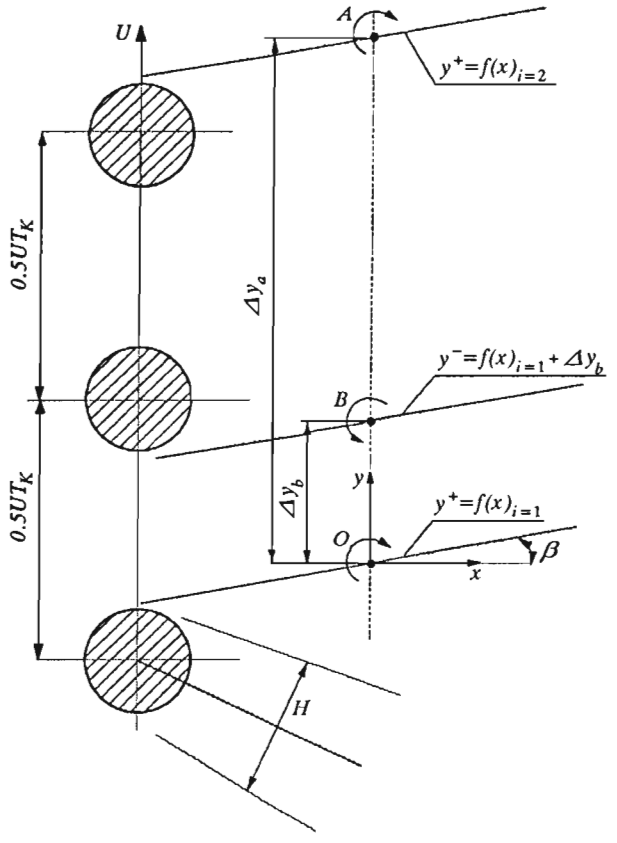

Fig. 3. A set of vortex trajectories behind moving cylinder

where $i = 1, 2, ...$ is the number of a consequtive pair of vortices, formed on the "upper" (y^+) and "lower" (y^-) sides of the cylinder respectively, and T_k denotes the Karman vortex period. The characteristic distances between particular trajectories (see Fig.3) may be found from the relationships

$$\begin{aligned} \Delta y_a &= y_{i+1}^+ - y_i^+ = UT_k = \frac{d}{\mathrm{St}\sqrt{1+\varphi^2}} \\ \Delta y_b &= y_i^- - y_i^+ = \frac{1}{2}UT_k - H\frac{\cos(\alpha+\beta)}{\cos\beta} = \\ &= \frac{d}{2\mathrm{St}\sqrt{1+\varphi^2}} - H\frac{\varphi^2(1-k)-k}{(1-k)\varphi\sqrt{1+\varphi^2}} \end{aligned} \tag{3.9}$$

The relations presented above prove that the distance Δy_a between two

consecutive trajectories of vortices forming on the same side of a moving cylinder is a function of Strouhal number St, cylinder diameter d and velocity ratio φ. On the other hand the distance Δy_b between trajectories of the vortices generated on the opposite sides of a cylinder depends additionally on a vortex path width H (Fig.2) and a convection velocity coefficient k.

A sample set of vortex trajectories plotted in Fig.3 exhibits moreover that the response of a hot-wire traversing the flow field in $x = \text{const}$ plane is undoubtedly under a strong impact of y-coordinate. In consequence, it seems reasonable to expect, that a phase-averaged velocity profile will depend also on the hot-sensor position with respect to the Karman vortex trajectories.

4. Experimental results and discussion

Theoretical predictions of the previous section could be experimentally verified with the use of the research facility described above. The experiment was performed at a constant jet velocity C for only one velocity ratio $\varphi = C/U = 1.0$. The Reynolds number, based on a rod diameter d and relative velocity W, was

$$\mathrm{Re} = \frac{Wd}{\nu} \simeq 2.2 \cdot 10^3$$

According to numerous opinions (cf Schlichting (1979)) this value of Re corresponds to the Strouhal number

$$\mathrm{St} = \frac{fd}{W} \simeq 0.2$$

So, an approximate distance between two corresponding vortex trajectories $\Delta y_a \to \Delta s_a$ may be estimated as

$$\Delta s_a = \frac{d}{\mathrm{St}\sqrt{1+\varphi^2}} \simeq 10.6\text{mm}$$

It should be emphasized here, that in order to maintain a constant rotational velocity U, the hot-wire probe had to be traversed along the arc s with the radius $R = R_0 + l/2$ (see Fig.1c) and not along the rectangular coordinate y (it proves the assumption $\Delta y \simeq \Delta s$).

The measurements were taken in 5 stations $x = \text{const}$, situated at the distances 5, 15, 25, 35 and 45 mm from the rotor, respectively. In the circumferential direction the probe traversed the flow field within the range

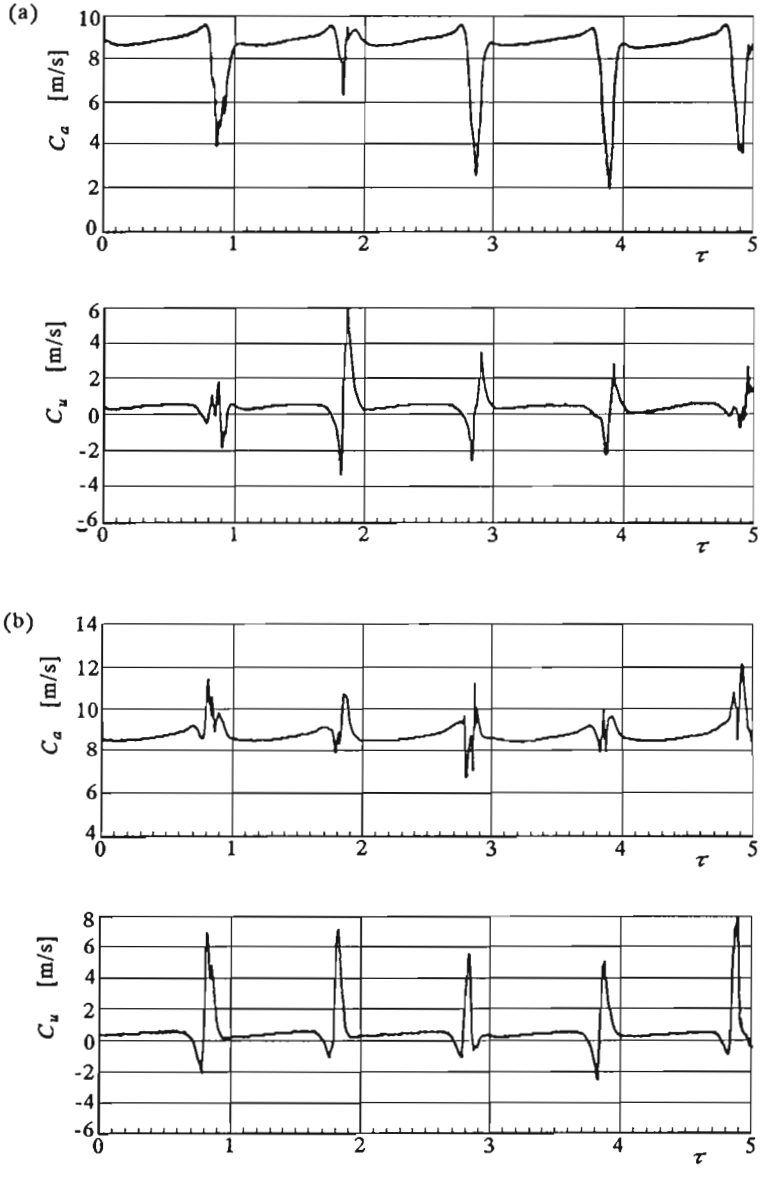

Fig. 4. Instantaneous velocity components recorded at two points: (a) – $x = 5$ mm, $s = 15$ mm; (b) – $x = 5$ mm, $s = 10$ mm

$s = \pm 20$ mm from the jet axis with the step $\Delta s = 1$ mm, so that the experimental grid points covered about four distances Δs_a calculated above.

An experimental implementation of the vortex pattern shown in Fig.3 demands a good correlation between the process of vortex formation and the instantaneous position of a moving cylinder. In other words, the "first" vortex behind each cylinder should always be generated at the same point of a flow field. The theoretical finding that the hot-wire response depends on its position with respect to vortex trajectories (see Fig.3) may easily be proved by the velocity time records plotted in Fig.4a and Fig.4b. They correspond to the same plane $x = \text{const}$ but are determined at 2 different points being $0.5\Delta s_a$ apart in s-direction. Even without any signal processing one can easily notice a significant divergence between the time-courses being compared, what is especially evident with reference to the axial velocity component C_a.

Fig.5 presents a spatial evolution of the periodic variance of axial velocity component $\overline{\tilde{C}_a^2}$. A visible periodicity in circumferential direction proves a strong impact of a vortex induced velocity field. The curves connecting corresponding peaks of $\overline{\tilde{C}_a^2}$ distribution, while projected on (x, s) plane, may be interpreted as lines parallel to vortex trajectories. As shown in Fig.6, the experimental points may be approximated with a good accuracy by parallel straight lines with a slope which appears to be $\tan\beta = 0.19$. The corresponding value of k-coefficient is now

$$k = \frac{\varphi \tan\beta}{1 + \varphi \tan\beta} \simeq 0.167$$

what is in a good agreement with its estimation found by other authors (cf Sallet (1957)). On the other hand, the constant value of k-coefficient provides an evidence, that according to Eq (3.5), the convection velocity of Karman vortices is also constant, at least within a flow region considered.

The spatial distribution of the periodic variance of circumferential velocity component $\overline{\tilde{C}_u^2}$ plotted in Fig.7 is less regular than that of its axial counterpart shown in Fig.5. The steep peaks observed at a first section $x = 5$ mm begin to merge pretty quickly in a downstream direction with a tendency to increase a circumferentially averaged $\overline{\tilde{C}_u^2}$-value. It is also worth noting that maxima of $\overline{\tilde{C}_a^2}$ correspond in a some measure to $\overline{\tilde{C}_u^2}$ minima.

Fig.8a and Fig.8b show the evolution of phase averaged velocity components $< C_a >$ and $< C_u >$ along the line 2 from Fig.6. It is conceivable that the maxima of $\overline{\tilde{C}_a^2}$ are associated with a relatively bad defect of phase averaged velocity $< C_a >$ which, however, tends gradually to vanish in the downstream direction. It is also worth noting that minima of $< C_a >$ profiles

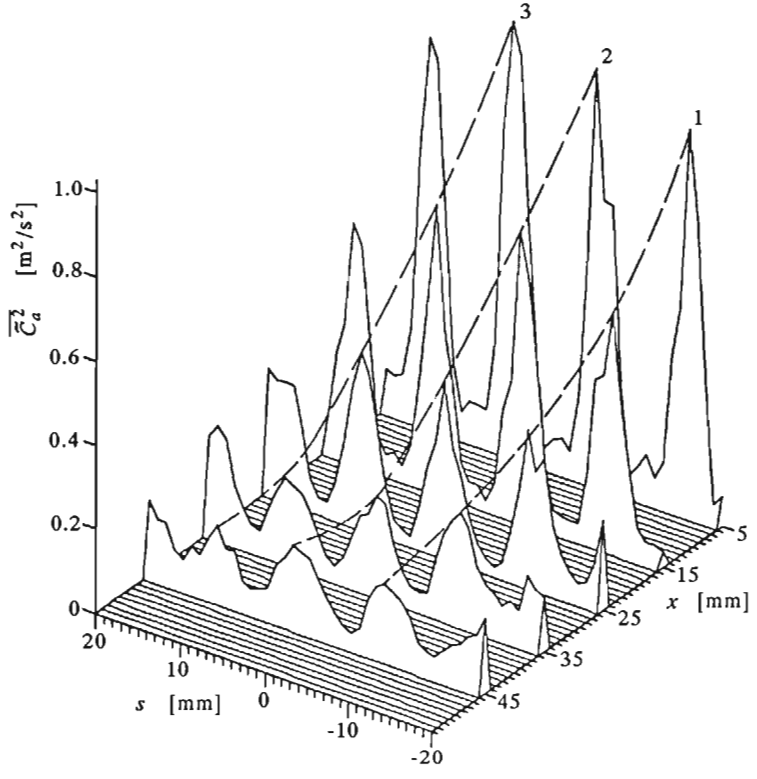

Fig. 5. Spatial evolution of $\overline{\tilde{C}_a^2}(x, s)$

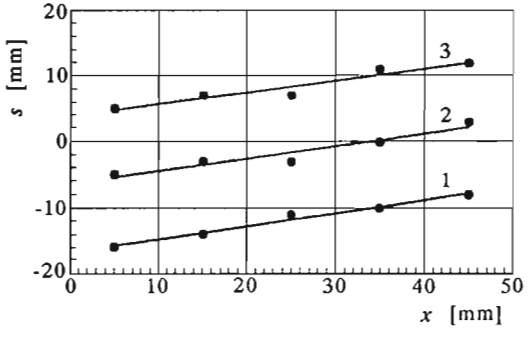

Fig. 6. Approximated lines connecting maxima of $\overline{\tilde{C}_a^2}$ – variance

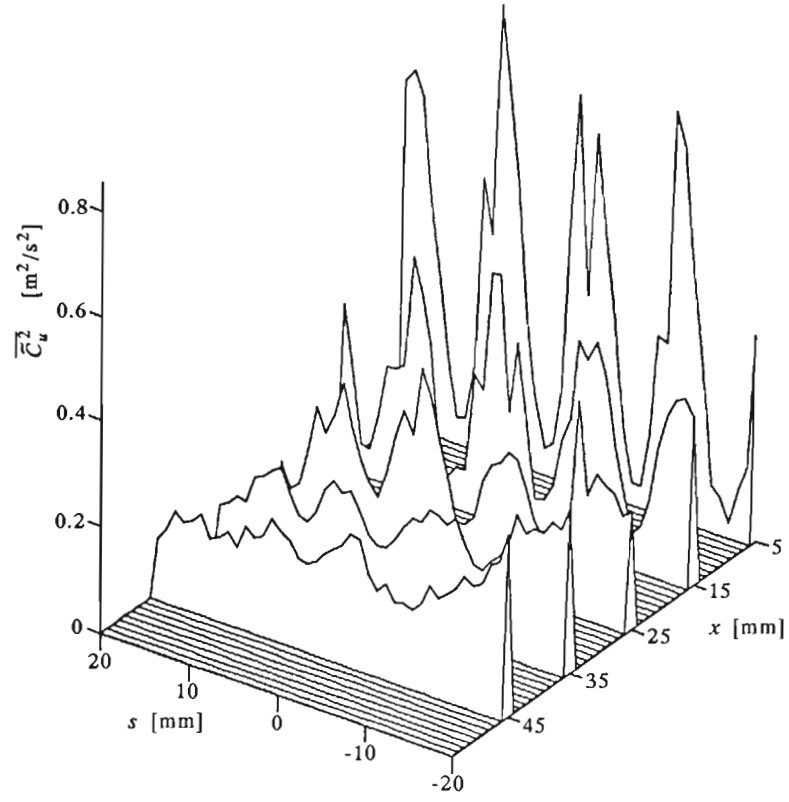

Fig. 7. Spatial evolution of $\overline{\tilde{C}_u^2}(x, s)$

coincide pretty well with a straight line what proves once more a constant value of convection velocity within a flow region considered.

The behaviour of the phase averaged circumferential velocity component $< C_u >$ is not so easy for interpretation. As can be seen (see Fig.8b), the $< C_u >$ component changes significantly its profile within the distance $x = 5 \div 15$ mm, but next it keeps a qualitatively similar shape up to $x = 45$ mm.

Fig.9a and Fig.9b present the phase averaged velocity components evaluated along the line corresponding to the minima of $\overline{\tilde{C}_a^2}$. Axial velocity component $< C_u >$ has now completely different character as compared with the profiles plotted in Fig.8a. There are no velocity defects typical for the wake flow pattern, what may be caused probably by a strong action of the vortex induced velocity field. On the contrary to the results presented in Fig.8b,

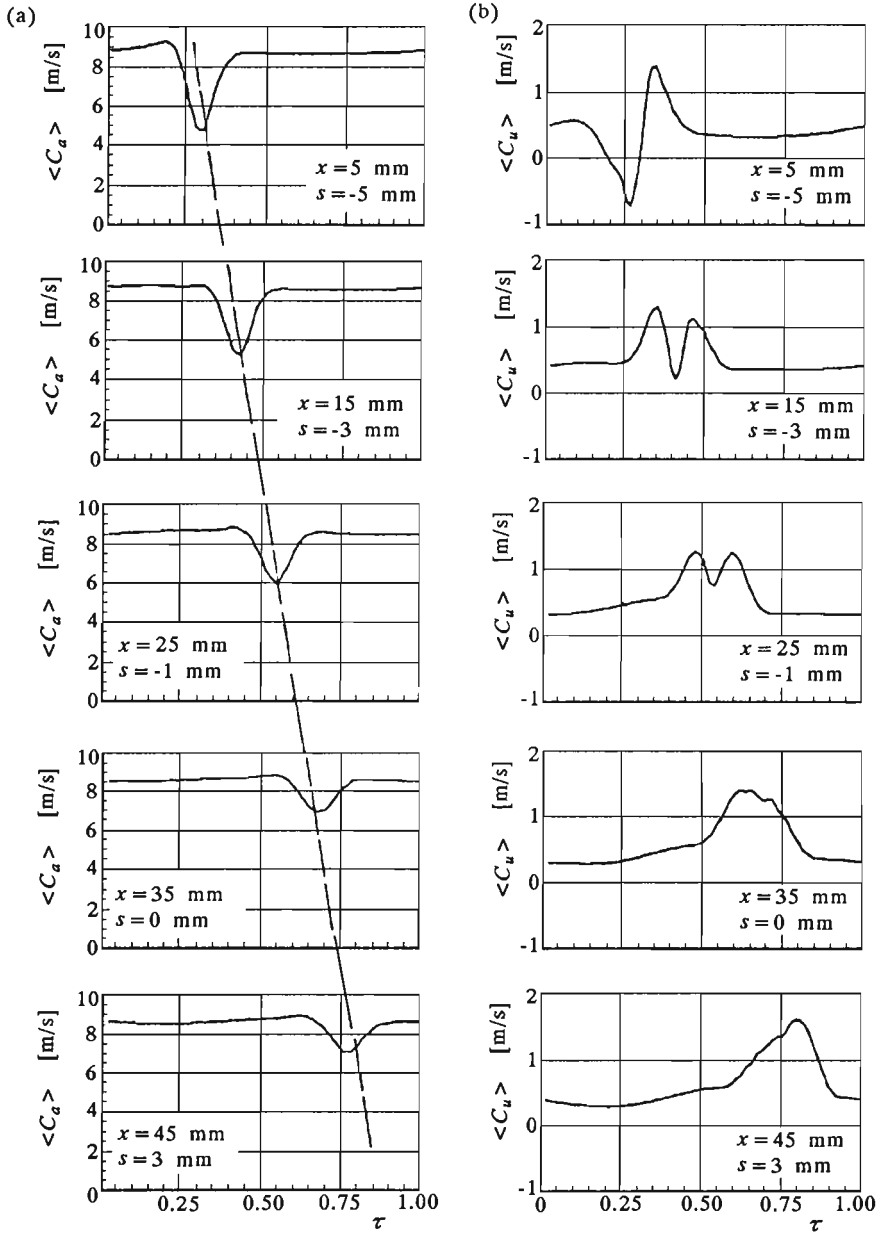

Fig. 8. Evolution of phase-averaged velocity profiles along the lines connecting maxima of $\overline{\tilde{C}_a^2}(x, s)$ – variance

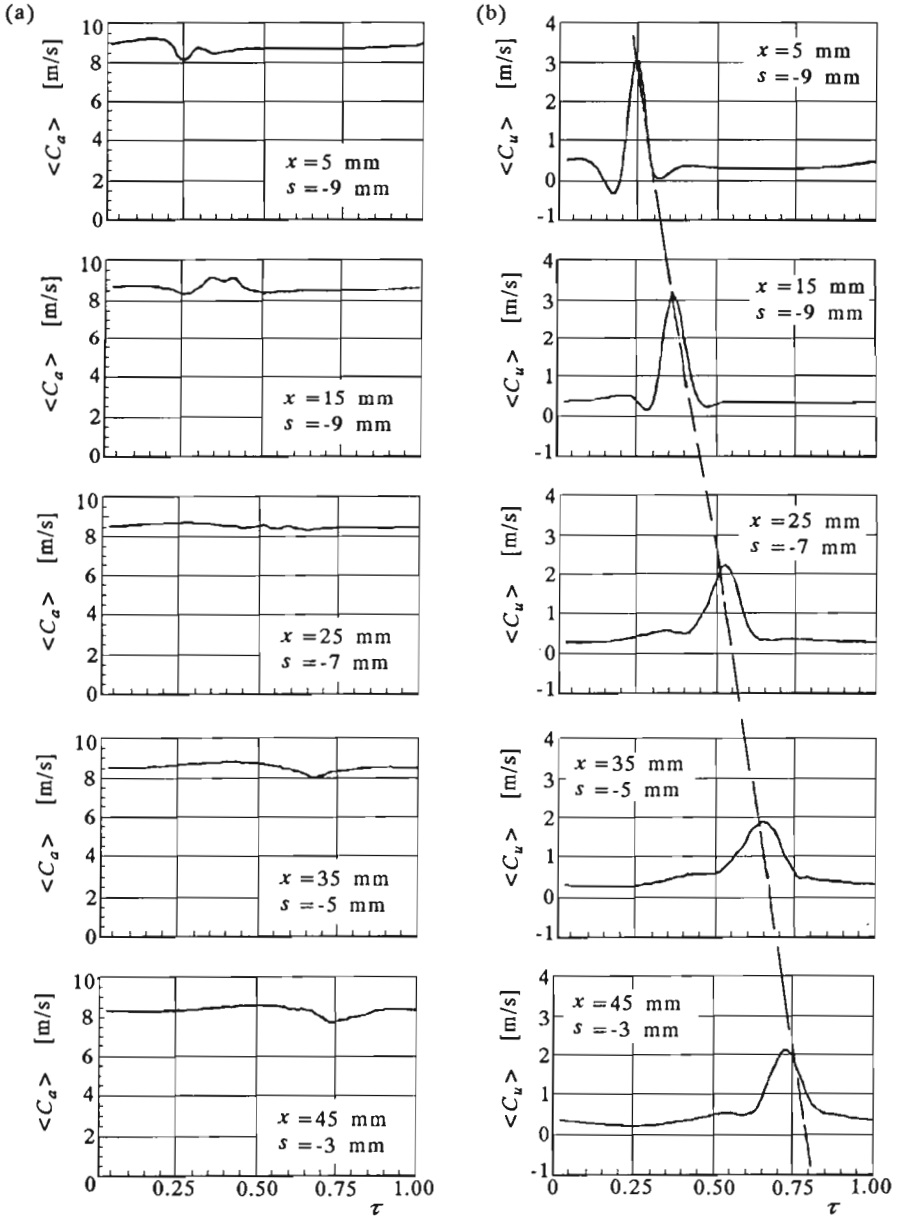

Fig. 9. Evolution of phase-averaged velocity profiles along the lines connecting maxima of $\overline{\widetilde{C}_u^2}(x,s)$ – variance

the behaviour of phase averaged circumferential velocity component $< C_u >$ seems to be in agreement with what should be expected.

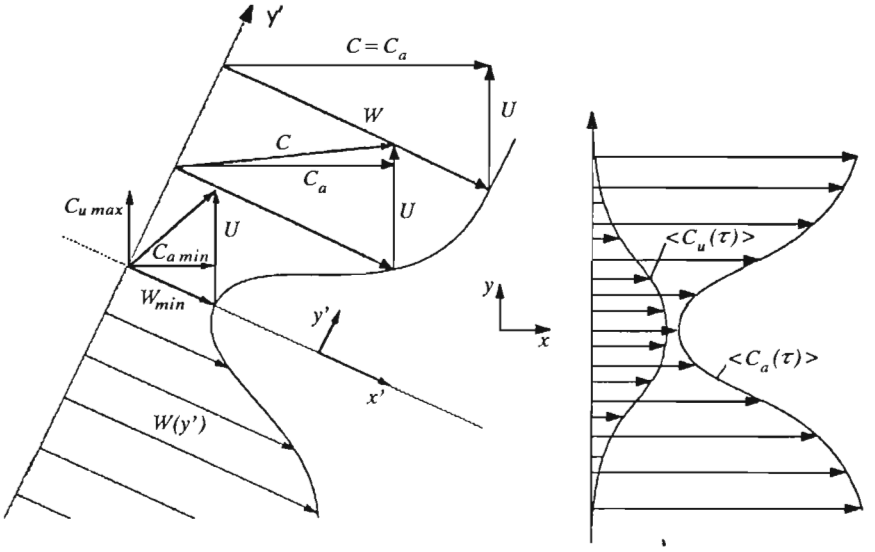

Fig. 10. Hypothetical phase-averaged velocity profile in a wakeflow behind moving streamlined body

If we take into account an ideal case of wakes traveling behind well-streamlined moving bodies which do not produce any vortex street, then we will obtain velocity distributions as given in Fig.10. As can be seen, the excess of $< C_u >$ velocity component corresponds here to the defect of axial velocity profile $< C_a >$. Such a picture would have been composed of Fig.8a and Fig.9b if each pair of velocity profile plotted there had been determined at one and the same point of the flow field.

5. Concluding remarks

The work presented here has a character of preliminary study, the more so, that the measurements have been taken for one velocity ratio $\varphi = C/U = 1.0$ and one Reynolds number only. Nevertheless, the results obtained so far suggest that in a case of a correlation between instantaneous cylinder position and the begining of the vortex street formation, the profiles of velocity components $< C_a >$ and $< C_u >$ are strongly affected by the velocity field induced by the

Karman vortex path. The preliminary velocity distributions in a moving wake are destroyed by the vortex action, so that in consequence the resultant phase averaged velocity profiles significantly depend on the measuring point position with respect to the vortex trajectories.

This work was sponsored by the polish State Committee for Scientific Research under grant KBN PB 201/3/91 No. 31019 91 01.

6. References

1. ELSNER J.W., 1987, *Turbulencja Przepływów,* PWN
2. GALLUS H.E., 1987, Unsteady Aerodynamic Measurements on Rotors, *AGARD-AG-298,* **1**
3. GREITZER E.M., 1985, An Introduction to Unsteady Flow in Turbomachines in Thermodynamics and Fluid Mechanics of Turbomachinery, *Proceedings of NATO Advanced Study Institute,* Martinus Nijhoss
4. GRIFFIN O.M., HALL M.S., 1991, Review-Vortex Shedding Lock-on and Flow Control in Bluff Body Wakes, *ASME Journal of Fluid Engineering,* **113**
5. GRIFFIN O.M., RAMBERG S.E., 1974, The Vortex-Street Wakes of Vibrating Cylinders, *J.Fluid Mech.,* **66**, 3
6. KIMURA T., TSUTAHARA M., WANG Z., 1992, Wake of a Rotating Circular Cylinder AIAA Journal, **30**, 2
7. MORKOVIN M.V., 1964, Flow Around Circular Cylinders: a Kaleidoscope of Challenging Fluid Phenomena, *Symp. on Fully Separated Flow, ASME*
8. SALLET D.W., 1957, The Drag and Oscillation Transverse Force on Vibrating Cylinders due to Steady Fluid Flow, *Ing.-Arch.,* **25**
9. SCHLICHTING H., 1979, *Boundary Layer Theory,* Mc Graw-Hill Book
10. SCHULZ H.D., GALLUS H.E., LAKSHMINARAYANA B., 1990, Three-Dimensional Separated Flow Field in the Endwall Region of an Annular Compressor Cascade in the Presence of Rotor-Stator Interaction: Part.1 – Quasi-Steady Flow Field and Comparison With Steady-State Data, Part.2 – Unsteady Flow and Pressure Field, *ASME Journal of Turbomachinery* **112**
11. WIERCIŃSKI Z., 1989, Geometria ścieżek wirowych za poruszającą się palisadą cylindrów, *Prace własne Instytutu Maszyn Przepływowych PAN*

Struktura śladu aerodynamicznego oraz geometria ścieżki wirowej za poruszającym się walcem kołowym

Streszczenie

Wpracy przedstawiono wyniki badań eksperymentalnych podjętych w celu wyjaśnienia mechanizmu wzajemnego oddziaływania ścieżki wirów Karmana oraz "lepkiego" śladu aerodynamicznego za poruszającym się walcem kołowym.

Manuscript received February 21, 1994; accepted for print April 27, 1994